DESIGN AND EXPERIMENT OF THE RECIPROCATING ADJUSTABLE STRIKING-VIBRATING COMBINED DEVICE for ROOT-SOIL SEPARATION of *GENTIANA*

/

往复调节式龙胆根土分离敲-振组合装置设计与试验

Hongguang CUI [1)], Guangshuo CHEN [1)], Zhanqiu XIE [1)], Wenzhong HUANG [2)], Weiming BIAN [2)], Liyan WU [1)], Cuihong LIU [1*)]

[1)] Shenyang Agricultural University, College of Engineering, Shenyang / China;

[2)] Fushun Agricultural and Rural Development Service Center, Fushun / China

Tel: +8615942060166; E-mail: cuihongliu77@syau.edu.cn

DOI: https://doi.org/10.35633/inmateh-74-80

Keywords: *Agricultural Machinery; Gentian; Root-Soil Separation; Crank Slider Mechanism; Reciprocating Adjustable mechanism; Striking-Vibrating Combination*

ABSTRACT

In order to solve the problem of low efficiency and potential damage in the separation of Gentiana roots from soil, a reciprocating adjustable striking-vibration combined device was designed, along with its performance testing. The ranges of working parameters for the vibration mechanism, striking mechanism, and adjustable reciprocating mechanism were determined through dynamic analysis of the mechanisms and materials. The effects of vibration frequency (X_1), crank speed (X_2), and screw feed speed (X_3) on the threshing efficiency (Y_1) and damage percentage (Y_2) were studied using a ternary quadratic regression orthogonal combination experimental method, combined with response surface analysis to explore the interaction effects of these factors on the indicators. A regression model was established through variance analysis. The significant factors affecting Y_1 were X_2, X_3, and X_1 in that order, while the significant factors affecting Y_2 were X_1, X_3, and X_2. In the interaction of factors, X_1X_2 significantly affected both Y_1 and Y_2; X_1X_3 had extremely significant impact on both Y_1 and Y_2; and X_2X_3 had extremely significant impact on Y_1. The optimal working parameters for the root-soil separation device of Gentian were determined to be vibration frequency of 6 Hz*, crank speed of 204* r/min*, and screw feed speed of 15* mm/s*. With this combination of parameters, experimental tests yielded a threshing efficiency of 90.8% and a damage percentage of 5.9%. The relative errors compared with the theoretical optimization results were less than 5%. This study meets requirements for the root-soil separation of Gentiana.*

摘要

为解决龙胆脱土效率低、易损伤的问题，设计了一种往复调节式敲-振组合的龙胆根土分离装置，并对其进行设计和性能试验。对敲击机构进行动力学分析，对龙胆根土复合体在振动筛上的受力进行分析，确定振动机构、敲击机构及调节式往复运动机构的工作参数范围。采用三元二次回归正交组合试验方法，以振动装置振动频率、敲击装置曲柄转速、调节式往复运动装置丝杠进给速度为试验因素，以脱净率、损伤率为试验指标，实施试验并对其结果进行分析，建立影响因素与评价指标回归模型。结果表明：龙胆根土分离装置最优工作参数为振动频率 6 Hz、曲柄转速 204 r/min、丝杠进给速度 15 mm/s，在此参数组合下进行试验台试验，得到龙胆根系脱净率为 90.8%，损伤率为 5.9%，与理论优化结果相对误差均小于 5%。能够满足龙胆根土分离田间作业要求。

INTRODUCTION

Gentiana (*Gentiana scabra Bunge*.) is a typical Chinese medicinal material, belonging to the Gentianaceae family of perennial herbs, and its rhizome is used medicinally for its effects in purging excessive fire from the liver and gallbladder (*Gao et al., 2020*). As an herbaceous root-type medicinal material, it is planted with a small spacing between plants, leading to a tangle of root systems from multiple plants in the later stages of growth. Compared to single-stemmed medicinal materials, the harvesting of *Gentiana* is challenging in terms of soil removal. During the harvesting process, it is difficult to achieve complete root-soil separation with field excavation and harvesting machinery, resulting in a large number of *Gentiana* root-soil complexes. Root-soil separation is an important post-harvest production step. Currently, farmers employ a significant labor force for manual separation of *Gentiana* roots and soil, which is labor-intensive, has low work efficiency, and is costly. Researching the mechanical separation of root-soil complexes for root-type medicinal materials, to achieve a higher root-soil threshing efficiency and lower root damage percentage during harvesting, is of great significance for the grading of medicinal materials, increasing the economic income of farmers, reducing the time for washing and drying medicinal materials, and minimizing the loss of effective components.

Overseas research on rhizome-type medicinal material harvesting and separation devices is relatively scarce, while numerous scholars in China have conducted relevant research on rhizome-type harvesting and separation devices and achieved certain results. For instance, *Liu Zhixin et al. (2024)* addressing the issues of separation damage in potato harvesters, designed a three-stage potato soil low-loss separation device, which was optimized through EDEM simulation to reduce the rate of damaged potatoes. *Yang Ranbing et al. (2024)* designed a low-damage fresh-eating sweet potato combine harvester based on a two-segment potato-soil separation device, which reduced the skin-breaking rate and impurity rate of sweet potato. *Liu Yafeng et al. (2024*) realized the harvesting and root-soil separation of rakkyo through roller differential crushing and brush-type conveying separation, which improved the root-soil separation rate and reduced the damage percentage. *Yan Shuai et al. (2023)* designed a drum-type experimental platform for separation of Codonopsis pilosula roots and soil, and through kinematic analysis, simulation analysis, and experimental platform testing, they optimized the design parameters of the root-soil separation device, achieving efficient damage reduction. *Tao Guixiang et al. (2022)* addressing the issues of low root-soil separation rate and high rhizome damage rate in the harvesting of Isatis indigotica, designed a combined oscillating type Isatis indigotica root-soil separation device, and through parameter optimization, enhanced the ability to crush and screen soil. *Chen Xueshen et al. (2015*) designed a two-roller root soil separation device for the root soil removal of Chinese medicinal material Polygonum cuspidatum. The team of *Zhang Zhaoguo* at Kunming University of Science and Technology has researched the Panax notoginseng harvesting and separation device, conducting an analysis of the working mechanism and parameter optimization of the Panax notoginseng harvester's conveying and separating device. They have used a secondary vibrating screen, a finger-like rubber lifting rod structure, and a two-stage lifting transmission method for the separation and cleaning of Panax notoginseng roots and soil (*Wang et al., 2023; Cui et al., 2018, Xue, 2022*).

Currently, traditional Chinese medicinal material harvesters have the advantages of high work efficiency and low energy consumption. However, due to the diversity of Chinese medicinal products, they are not suitable for the separation and harvesting of the root-soil complex of *Gentiana* (RSCG), which have dense and intertwined root systems and soil. In this paper, a root-soil separation device targeting RSCG is developed, which combines striking and vibration separation methods and is equipped with an adjustable reciprocating mechanism. This allows the striking mechanism to descend with the height reduction of the root-soil complex, thereby improving work efficiency and soil threshing efficiency, reducing root damage percentage, and enhancing the quality of operation. Through dynamic analysis, key components are designed and parameters are selected. Orthogonal tests are conducted on the prototype's threshing efficiency and damage percentage to seek optimal working parameter combinations, aiming to provide technical references for the mechanized root-soil separation of *Gentiana*.

MATERIALS AND METHODS

Mechanism design and working principle

The root-soil separation device of *Gentian* is primarily composed of three parts: the striking mechanism, the vibrating mechanism, and the adjustable reciprocating mechanism. The striking mechanism and the vibrating mechanism are driven by crank-slider mechanisms, while the adjustable reciprocating mechanism is driven by a ball screw. The structural diagram is illustrated in Figure 1.

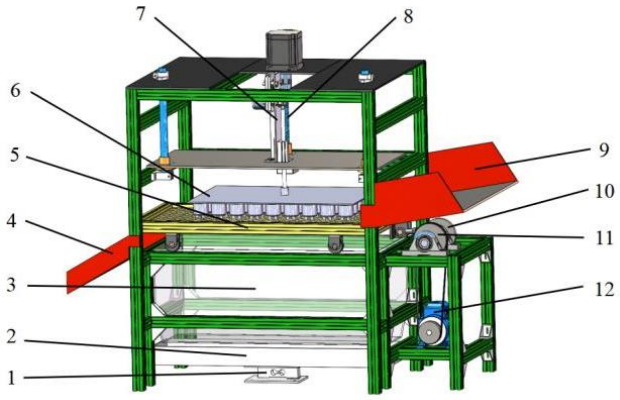

Fig. 1 - Structure diagram of root-soil separation device of Gentian

1-Weighing sensor; 2- Soil weighing tray; 3- Soil retaining box; 4- Discharge outlet; 5- Vibrating screens; Striking plate; 7- Striking mechanism; 8- Adjustable reciprocating mechanism; 9- Feed Inlet 10- Eccentric Wheel; 11- Belt Pulley; 12- Electric Motor

Working principle

The incompletely separated RSCG scattered in the field after the field harvester's operation are placed on the vibrating screen of the root-soil separation device of *Gentian* through the feed inlet. The striking mechanism drives the striking plate to hit RSCG, while the adjustable reciprocating mechanism moves downward at a preset speed, achieving dynamic adjustment of the distance between the striking plate and RSCG as their height decreases. Under the reciprocating vibration of the vibrating mechanism, the crushed soil falls through the mesh holes of the vibrating screen into the soil weighing tray, while the gentian roots, being larger than the diameter of the mesh holes, remain on the surface of the vibrating screen. Driven by the friction force of the vibrating screen, the *Gentian* roots move towards the discharge outlet, thereby achieving the separation of *Gentian* roots and soil. With the reciprocating motion of the striking mechanism, a large quantity of Gentian can be processed, enhancing work efficiency and saving labor, while achieving better processing results for RSCG.

Design of Striking Mechanism

Due to its ability to achieve reciprocating striking motion, simple structure, easy processing, and good adjustability of follower motion laws, the crank-slider mechanism is selected as the driving mechanism for the striking mechanism. The schematic diagram of the mechanism is shown in Figure 2, where *AB* represents the crank, *BC* represents the connecting rod, and the rectangle represents the striking plate *C*. During operation, the crank-slider mechanism *ABC* reciprocates under the rotation of the crank, causing the striking plate *C* to reciprocate and tap RSCG on the vibrating screen, thereby separating the *Gentian* roots from the soil aggregates. The structure and operating parameters of the crank-slider mechanism directly affect the striking effect, which is analyzed specifically in this paper.

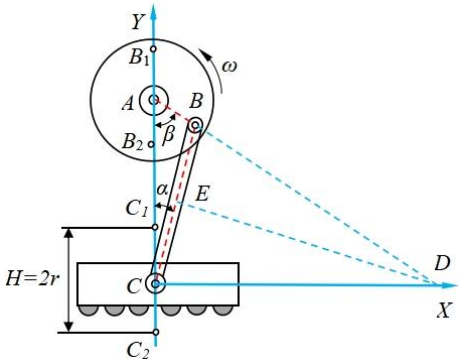

Fig. 2 - Schematic diagram of Crank slider mechanism

A rectangular coordinate system is established with the origin at point *A*, which is the rotary center of the crank in Figure 2, and with the frame *AC* collinear with the Y-axis. The angles *α* and *β* represent the angles between *BC* and the Y-axis, and *AB* and the Y-axis, respectively (*Feng et al., 2023; Luo et al., 2018, Tang et al., 2020*). Point *E* is the midpoint of the connecting rod *BC*, while Point *D* is the instantaneous center of velocity for the connecting rod *BC*. Therefore, the trajectory coordinates of the points *C* is $y_C=y_B-l_{BC}\cos\alpha$.

Due to the limitations of the frame's spatial structure and the installation position of the striking mechanism, the initial length range of the crank is determined to be 40 mm ≤ l_{AB} ≤ 50 mm, and the connecting rod length l_{BC} is 85 mm. Establish the velocity equation of the striking mechanism's motion. Given the displacement equation of the striking mechanism, the first derivative of displacement with respect to time is velocity. By taking the first derivative of the displacement equation, the velocity of point *C* can be obtained.

$$Y_C' = l_{AB} \cdot l_{BC}(\beta' \sin\beta\cos\alpha + \alpha' \sin\alpha\cos\beta) \quad (1)$$

Establish the acceleration equation for the striking mechanism's motion. According to the first derivative of displacement with respect to time being velocity, and the second derivative being acceleration. Solve the second derivative of equation (1) to obtain the acceleration at point C.

$$Y_C'' = l_{AB} \cdot l_{BC}[(\alpha'^2 + \beta'^2)\cos\alpha\cos\beta - 2\alpha'\beta' \sin\alpha\sin\beta] \quad (2)$$

From the acceleration formula (2), it can be seen that the acceleration of the striking mechanism is related to the rotational speed of crank and the lengths of l_{AB} and l_{BC} (*Zou, 2023; Lu, 2022*).

The angular velocity of the crank *AB* is ω_A, the angular velocity of the connecting rod *BC* is ω_C, and the angular velocity of the instantaneous center of velocity D is ω_D. According to the kinematic principles of plane motion of a rigid body, it can be derived:

$$v_B = l_{AB}\omega_A \tag{3}$$

$$\omega_D = \frac{v_B}{l_{BD}} = \frac{l_{AB}\cdot\omega_A}{l_{BD}} \tag{4}$$

$$v_C = l_{CD}\omega_D = \frac{l_{CD}\cdot l_{AB}\cdot\omega_A}{l_{BD}} \tag{5}$$

Let the moment of inertia of AB about point A be J_1, and the moment of inertia of BC about its centroid E be J_2. The moment of inertia of *BC* about its instantaneous center of velocity D is J_C, according to the kinetic energy theorem, the total kinetic energy of this system of particles is:

$$T = T_{AB} + T_{BC} + T_C \tag{6}$$

where: $T_{AB} = \frac{1}{2}J_1\omega_A^2$, $T_{BC} = \frac{1}{2}m_{BC}v_E^2 + \frac{1}{2}J_C\omega_E^2$, $T_C = \frac{1}{2}m_C v_C^2$, substituting T_{AB}, T_{BC} and T_C into equation (6) yields

$$T = \frac{1}{2}J_1\omega_A^2 + \frac{1}{2}m_{BC}v_E^2 + \frac{1}{2}J_C\omega_E^2 + \frac{1}{2}m_C v_C^2 \tag{7}$$

where: $v_E = \omega_D \cdot l_{DE}$, $\omega_E = \frac{2v_E}{l_{BC}}$, $J_1 = \frac{1}{3}m_{AB}l_{AB}^2$, $J_C = \frac{1}{12}m_{BC}l_{BC}^2$.

The soil crushing by striking is an instantaneous collision process, and the collision process always satisfies the law of conservation of energy, neglecting the work done by the impact force generated during the collision process in the direction of deformation of RSCG and the energy consumed by the frictional force of the mechanism (*Qian*, *2015*; *Zhao et al.*, *2013*). Based on the previous impact test of RSCG, the striking energy is determined to be 1.4 J. According to the kinetic energy theorem for the system of particles, the formula is obtained:

$$\Delta E_k = C \tag{8}$$

$$\Delta E_k = T_{AB} + T_{BC} + T_C \tag{9}$$

When the angle β is 45°, the range of the crank length is 40 mm≤l_{AB}≤50 mm, and the length of the connecting rod is 85 mm. The masses of the crank, connecting rod, and striking plate are measured to be 0.01 kg, 0.06 kg, and 3 kg, respectively. Substituting these values, the range of the crankshaft speed is calculated to be 168 r/min≤n≤240 r/min.

Design of Vibrating Mechanism

The vibration mechanism is shown in Figure 3. Under the drive of the motor, the crank disc performs uniform circular motion, which leads the connecting rod to move periodically. Through the action of the connecting rod on the vibration screen, the screen surface is driven to move periodically. This causes RSCG to move back and forth in front of the screen, with the forward movement distance being greater than the backward movement distance. This ensures that RSCG moves from the material feed inlet to the material discharge outlet (*Li et al., 2024*), thereby achieving the planar reciprocating vibration of the vibration screen. The struck root-soil complex of *Gentian* is affected by the vibration frequency of the vibration mechanism during the movement of the sieve mesh. If the vibration frequency is too low, RSCG cannot generate relative motion with the sieve mesh. The soil that is struck and falls cannot spread out on the sieve surface, preventing the separation of the *Gentiana* root system from the soil. If the vibration frequency is too high, RSCG moves too quickly on the sieve mesh, leading to RSCG being carried away without sufficient screening. Both excessively low or high vibration frequencies can result in poor screening effects. Therefore, designing reasonable parameters for the vibration mechanism is crucial for improving the soil removal effect.

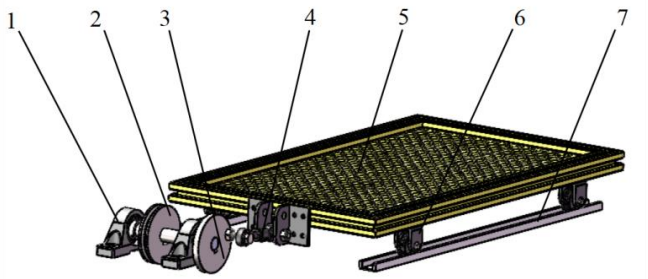

Fig. 3 - Structure diagram of Vibrating mechanism

1- Bearing housing; 2- Pulleys; 3- Crank disc; 4- Connecting rod; 5- Sieve body; 6- Sieve wheel; 7- Track

Motion Analysis of RSCG

The main form of motion for RSCG on the screen surface is the reciprocating motion of the composite along the screen surface. The reciprocating motion of RSCG along the screen surface is related to the frictional forces between the composite and the screen surface, as well as the composite and the striking plate. In order to continuously direct RSCG towards the discharge outlet, the force propelling the composite towards the discharge outlet along the screen surface must be greater than the force pushing it towards the feed inlet. To improve the screening efficiency, it is necessary to increase the distance RSCG travels on the screen surface. Therefore, the composite must be able to move along the screen surface towards the feed inlet. The force analysis of RSCG's motion on the screen surface is shown in Figure 4 (*Cui et al., 2021*).

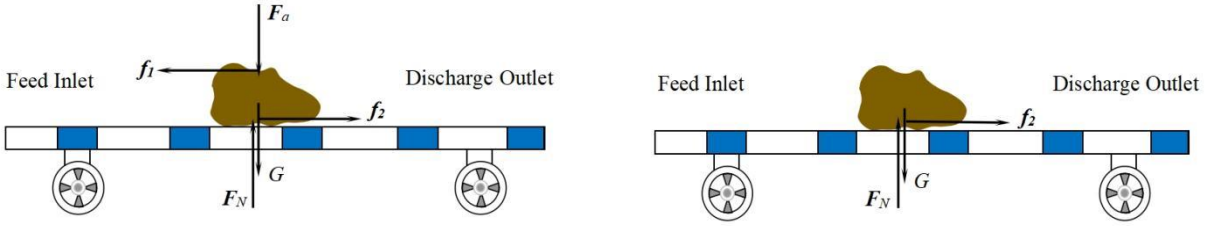

a. RSCG Subjected to Striking Force b. RSCG Not Subjected to Striking Force

Fig. 4 - Force analysis diagrams of RSCG along the screen

Note: F_N represents the supporting force of the screen surface on the material, N; F_a represents the striking force of the striking plate on the material, N; f_1 represents the frictional force of the striking plate on the material, N; f_2 represents the frictional force of the screen surface on the material, N; G represents the material gravity, N.

The motion of RSCG includes movement from the feed inlet to the discharge outlet of the vibrating screen, as well as root-soil separation (*Wei et al., 2019, Wei et al., 2023, Lv et al., 2022, Wei et al., 2018*). When the vibrating screen is not subjected to vibration, the shape of its screen surface can be approximated to a straight line *(Quan et al., 2013)*. RSCG is considered as a rigid body. If air resistance is neglected, the force analysis is shown in Figure 4. When RSCG is subjected to a striking force, f_2 is the resistance for the composite to move towards the feed inlet. The dynamic equation in this state is:

$$f_1 - f_2 = ma_{x1} \tag{10}$$

$$f_1 = \mu_1 F_a \tag{11}$$

$$f_2 = \mu_2 F_N \tag{12}$$

$$F_N = F_a + G \tag{13}$$

$$f_2 = ma_0 = mA\omega^2 \cos(\omega t) \tag{14}$$

where: m is the mass of RSCG, kg; g is the acceleration due to gravity, taken as 9.8 m/s^2; μ_1 is the coefficient of friction between the striking plate and RSCG; μ_2 is the coefficient of friction between the screen surface and RSCG; a_{x1} is the tangential acceleration of RSCG when subjected to the striking force, m/s^2.

Substitute equations (11) and (14) into equation (10) and then rearrange to obtain.

$$\mu_1 F_a - mA\omega^2 \cos(\omega t) = ma_{x1} \tag{15}$$

Similarly, when RSCG is not subjected to a striking force, f_2 is the driving force for the composite to move towards the discharge opening. The dynamic equation in this state is:

$$f_2 = ma_{x2} \tag{16}$$

$$f_2 = ma_0 = mA\omega^2 \cos(\omega t) \tag{17}$$

$$f_2 = \mu_2 F_N \tag{18}$$

$$F_N = G \tag{19}$$

Collation available:

$$mA\omega^2 \cos(\omega t) = ma_{x2} \tag{20}$$

where: a_{x2} represents the tangential acceleration of RSCG when it is not subjected to a striking force, m/s^2.

Analysis indicates that the reciprocating motion of RSCG along the screen surface is related to the screen vibration amplitude *A*, the rotational angular velocity of the crank disc *ω*, the mass of RSCG *m*, and the frictional force experienced by RSCG *a*. The back-and-forth motion of RSCG on the vibrating screen can extend the travel distance of the composite on the screen surface, which is beneficial for root-soil separation. When RSCG is subjected to a striking force, it moves along the screen surface towards the feed inlet; reducing the screen vibration amplitude *A* and increasing the rotational angular velocity of the crank disc *ω* are beneficial for the movement of RSCG towards the feed inlet. Similarly, when RSCG is not subjected to a striking force, it moves along the screen surface towards the discharge outlet; increasing the screen vibration amplitude *A* and decreasing the rotational angular velocity of the crank disc *ω* are beneficial for the movement of RSCG towards the discharge outlet. Preliminary tests have determined that when the vibration frequency of the vibrating screen is within the range of 4 Hz to 8 Hz, the *Gentiana* root system after soil removal can move along the screen surface towards the discharge outlet.

Adjustable reciprocating mechanism

The adjustable reciprocating mechanism is composed of a ball screw pair, with the purpose of adjusting the distance between the striking plate and RSCG. As RSCG is reduced in size by the striking plate, if the striking plate always remains stationary, it would result in the striking plate being unable to strike RSCG. The role of the ball screw is to dynamically adjust the distance between the striking plate and RSCG. The adjustable reciprocating mechanism is shown in Figure 5.

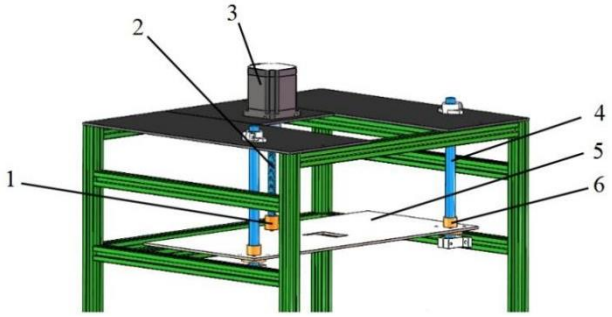

Fig. 5 - Structure diagram of Adjustable reciprocating mechanism

1. Optic axis; 2- Stepping motor; 3- Ball screw; 4- Nut; 5- Carrier platforms; 6- Ball round flange linear bearings

By calculation, the range of the crankshaft speed is determined to be 168 r/min≤n≤240 r/min. Taking the midpoint of the crankshaft speed, *n*=204 r/min, it is found that the time required for the striking mechanism to strike once is 0.3 seconds. Through preliminary impact tests, the average range of height difference Δh is determined to be 3.07 mm to 6.03 mm. Calculations are performed using equation (21), the range of the descending speed for the adjustable reciprocating mechanism is determined to be 10~20 mm/s.

$$v = \frac{\Delta h}{t} \tag{21}$$

where: v is the descending speed of the lead screw, mm/s; Δh is the average height difference of RSCG, mm; t is the time for the striking mechanism to strike once, s.

Experiment design

Experiment condition and equipment

The experimental site is the laboratory of the College of Engineering at Shenyang Agricultural University. The experimental materials are sourced from the *Gentiana* planting base in Qingyuan Manchu Autonomous County, Fushun City. To adapt to the root-soil separation device and operational requirements, the stems and leaves of the *Gentiana* are removed before the experiment, and the root blocks are divided into appropriately sized root-soil complex. The experimental method refers to GB/T5667-2008 "Agricultural Machinery Production Test Methods." The test indicators are the threshing efficiency and damage percentage of the *Gentiana* root system. Natural air drying is utilized to maintain the moisture content of the *Gentiana* root-soil composite between 10% and 15%.

Main experimental equipment and instruments: root-soil separation device of Gentian test bench, one laptop computer, a laser tachometer (range 1–9999 r/min, accuracy ±0.02%), a weighing sensor (range 50 kg, accuracy 0.02 kg), a multifunctional electronic stopwatch, and a steel tape measure (range 3 m, accuracy 1 mm), as shown in Figure 6.

Fig. 6 - Test bench for root-soil separation of *Gentiana*

1- High-speed camera; 2- Real-time weight detection system for detached soil;
2- Striking mechanism; 4- Vibrating mechanism; 5- Adjustable reciprocating mechanism

Experiment factors and indexes

Based on the results of single-factor experiments and the design of mechanisms, it has been determined that the vibration frequency (X_1), crank speed (X_2), and screw feed speed (X_3) are the three most significant factors affecting the performance of the root-soil separation device of *Gentian*, and the range of levels for the test factors has been established. According to the Box-Behnken three-factor three-level experimental design in Design-Expert 12.0 software, the work performance of the root-soil separation device of *Gentian* was studied, with the root threshing efficiency and damage percentage as the response values. The levels of the test factors are shown in Table 1. The main indicators for evaluating the efficiency of the root-soil separation of *Gentiana* are the threshing efficiency and damage percentage of the Gentiana root system, and the calculation formulas for the evaluation indicators are shown in equations (22) and (23).

$$Y_1 = \frac{m_0 - m_1}{m_0 - m_2} \times 100\% \quad (22)$$

$$Y_2 = \frac{m_3}{m_2} \times 100\% \quad (23)$$

where: Y_1 is the threshing efficiency of Gentian roots, %; Y_2 is the damage percentage of Gentian root system, %; m_0 is the total mass of RSCG before the test, kg; m_1 is the total mass of RSCG after the test, kg; m_2 is the total mass of the net root system without residual soil, kg; m_3 is the mass of damaged Gentian roots after root-soil separation, kg.

Table 1

Factors and levels of combination experiment

Levels	Factors		
	Vibration frequency	Crank speed	Screw feed speed
	[Hz]	[r·min^{-1}]	[mm·s^{-1}]
	X_1	X_2	X_3
-1	4	168	10
0	6	204	15
1	8	240	20

RESULTS

The orthogonal test plan includes 17 test points, among which there are 12 analysis factors and 5 zero-point estimation errors. The test design scheme and test results are shown in Table 2. Based on the experimental data in Table 2, the Design-Expert 12.0 software is used to perform a multivariate regression fitting analysis on the experimental data, establishing a second-order polynomial regression model for the test indicators of *Gentiana* root threshing efficiency Y_1 and damage rate Y_2 against the three test factors of vibration frequency X_1, crank speed X_2, and screw feed speed X_3.

Table 2

Experimental plan and results

No.	Vibration frequency [Hz]	Crank speed [r·min^{-1}]	Screw feed speed [mm·s^{-1}]	Y_1 [%]	Y_2 [%]
1	-1	1	0	91.7	6.1

No.	Vibration frequency [Hz]	Crank speed [r·min^{-1}]	Screw feed speed [mm·s^{-1}]	Y_1 [%]	Y_2 [%]
2	0	0	0	94.9	3.7
3	0	0	0	94.7	3.5
4	-1	0	-1	91.6	5.6
5	1	0	1	91.6	5.4
6	1	-1	0	92.8	4.5
7	1	0	-1	92.9	3.9
8	0	0	0	94.3	3.4
9	-1	0	1	94.4	5.2
10	-1	-1	0	93.9	4.8
11	0	-1	1	94.1	5.3
12	1	1	0	92.2	4.6
13	0	1	1	91.7	5.7
14	0	0	0	94.4	3.3
15	0	-1	-1	92.1	4.6
16	0	0	0	94.8	3.6
17	0	1	-1	92.2	4.6

Experiment results variance analysis

According to the analysis of variance results in Table 3, it can be seen that the model *P* for the threshing efficiency (Y_1) and damage percentage (Y_2) are both significantly less than 0.01, and the *P* for the lack of fit are both significantly greater than 0.05. The model determination coefficients R^2 are 0.9847 for the threshing efficiency and 0.9764 for the damage percentage. In summary, it can be concluded that the regression model is significant and has a good fit, making the model reliable.

Table 3

Data significance experiment and analysis of variance

Source of variation	The threshing efficiency Y_1					The damage percentage Y_2				
	SS	DF	MS	*F* value	*P* value	SS	DF	MS	*F* value	*P* value
Model	25.77	9	2.86	50.04	<0.0001**	12.33	9	1.37	32.24	<0.0001**
X_1	0.5512	1	0.5512	9.63	0.0172*	1.36	1	1.36	32.03	0.0008**
X_2	3.25	1	3.25	56.83	<0.0001**	0.4050	1	0.4050	9.53	0.0176*
X_3	1.13	1	1.13	19.66	<0.0030**	1.05	1	1.05	24.74	0.0016***
X_1X_2	0.6400	1	0.6400	11.19	0.0123*	0.3600	1	0.3600	8.47	0.0226*
X_1X_3	4.20	1	4.20	73.45	<0.0001**	0.9025	1	0.9025	21.24	0.0025*
X_2X_3	1.56	1	1.56	27.31	<0.0012**	0.0400	1	0.0400	0.9412	0.3643
X_1^2	3.68	1	3.68	64.34	<0.0001**	2.29	1	2.29	53.89	0.0002**
X_2^3	4.51	1	4.51	78.83	<0.0001**	2.45	1	2.45	57.60	0.0001**
X_3^2	4.73	1	4.73	82.69	<0.0001**	2.61	1	2.61	61.44	0.0001**
Residual	0.4005	7	0.0572			0.2975	7	0.0425		
Lack of Fit	0.1325	3	0.0442	0.6592	0.6187	0.1975	3	0.0658	2.63	0.1864
Pure error	0.2680	4	0.0670			0.1000	4	0.0250		
Total sum	26.17	16				12.63	16			

On the basis that the model is significant without loss of fitting, the non-significant terms in the model are eliminated, and the regression equation is obtained, as shown in equations (24) and (25).

$$Y_1=94.62-0.263X_1-0.638X_2+0.375X_3+0.4X_1X_2-1.03X_1X_3-0.625X_2X_3-0.935X_1^2-1.04X_2^2-1.06X_3^2 \quad (24)$$

$$Y_2=3.50-0.413X_1+0.225X_2+0.363X_3-0.3X_1X_2+0.475X_1X_3+0.1X_2X_3+0.738X_1^2+0.763^2+0.788X_3^2 \quad (25)$$

Analysis of influencing factors

The response surface plots were obtained using Design-Expert 12.0 software as shown in Figure 7, which further investigate the impact patterns of the test factors (vibration frequency, crank speed, and screw feed rate) and their interactions on the test indicators (threshing efficiency Y_1 and damage percentage Y_2).

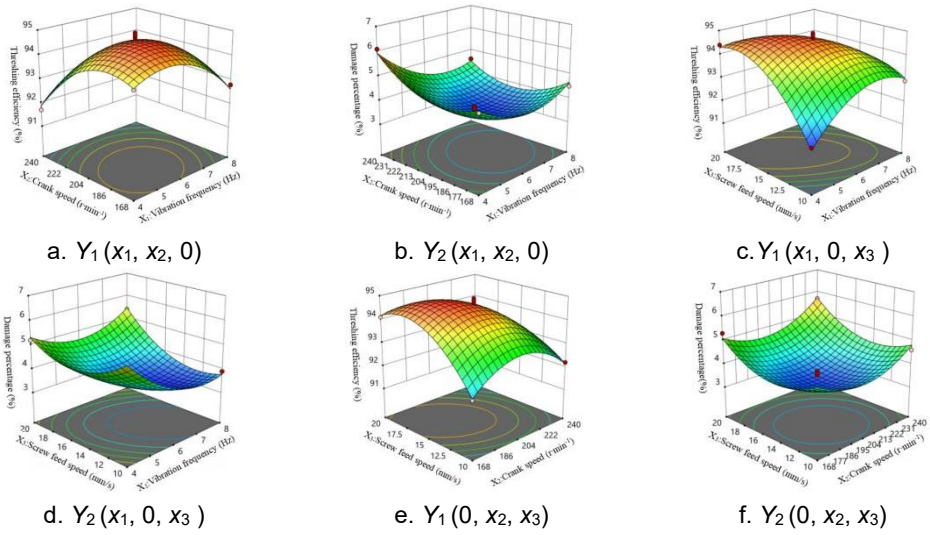

a. Y_1 (x_1, x_2, 0) b. Y_2 (x_1, x_2, 0) c. Y_1 (x_1, 0, x_3)

d. Y_2 (x_1, 0, x_3) e. Y_1 (0, x_2, x_3) f. Y_2 (0, x_2, x_3)

Fig. 7 - Response surface analysis of the factors' interaction effect on the index

Figures 7a and 7b are the response surface plots showing the interactive effects of vibration frequency (X_1) and crank speed (X_2) on the threshing efficiency (Y_1) and damage percentage (Y_2). The interaction is significant. When the vibration frequency ranges from 4 to 8 Hz and the crank speed ranges from 168 to 240 r/min, the threshing efficiency is relatively optimal and the damage percentage is relatively low. When the screw feed speed (X_3) is at the central level (X_3 = 15 mm/s), at a given vibration frequency, the threshing efficiency first increases and then decreases with the increase of the crank speed, showing a significant change; the damage percentage first decreases and then increases with the increase of the crank speed, showing a significant change; when the crank speed is constant, the threshing efficiency first increases and then decreases with the increase of the vibration frequency, and the change amplitude is higher than the influence of the crank speed change. The damage percentage first decreases and then increases with the increase of the vibration frequency, and the change amplitude is lower than the influence of the crank speed change.

Figures 7c and 7d are the response surface plots showing the interactive effects of vibration frequency (X_1) and screw feed speed (X_3) on the threshing efficiency (Y_1) and damage percentage (Y_2). The interaction is significant. When the screw feed speed ranges from 10 to 20 mm/s and the vibration frequency ranges from 4 to 8 Hz, the threshing efficiency is relatively optimal and the damage percentage is relatively low. When the crank speed (X_2) is at the central level (X_2 = 204 r/min), at a given screw feed speed, the threshing efficiency first increases and then decreases with the increase of the vibration frequency, showing a significant change; the damage percentage first decreases and then increases with the increase of the vibration frequency, showing a significant change; when the vibration frequency is constant, the threshing efficiency first increases and then decreases with the increase of the screw feed speed, and the change amplitude is significantly higher than the influence of the vibration frequency change; the damage percentage first decreases and then increases with the increase of the screw feed speed, and the change amplitude is significantly lower than the influence of the vibration frequency change.

Figures 7e and 7f are the response surface plots showing the interactive effects of crank speed (X_2) and screw feed speed (X_3) on the threshing efficiency (Y_1). The interaction is significant. When the screw feed speed ranges from 10 to 20 mm/s and the crank speed ranges from 168 to 240 r/min, the threshing efficiency is relatively optimal and the damage percentage is relatively low. When the vibration frequency (X_1) is at the central level (X_1 = 6 Hz), at a given screw feed speed, the threshing efficiency first increases and then decreases with the increase of the crank speed, showing a significant change; the damage percentage first decreases and then increases with the increase of the crank speed, showing a significant change; when the crank speed is constant, the threshing efficiency first increases and then decreases with the increase of the screw feed speed, and the change amplitude is significantly higher than the influence of the crank speed change; the damage percentage first decreases and then increases with the increase of the lead screw feed speed, and the amplitude change is slightly higher than the influence of the crank speed change.

Parameter optimization and verification test

Utilizing Design-Expert 12.0 software to conduct target optimization for the parameter combination of the root-soil separation device of Gentian, based on the working conditions of the root-soil separation device

of Gentian and the variance analysis results of the root threshing efficiency and damage percentage, the parameter optimization constraints are determined as.

$$\begin{cases} \max Y_1(X_1, X_2, X_3) \\ \\ \min Y_2(X_1, X_2, X_3) \\ s.t. \begin{cases} 4 \le X_1 \le 8 \\ 168 \le X_2 \le 240 \\ 10 \le X_3 \le 20 \end{cases} \end{cases} \quad (26)$$

After analysis with Design-Expert 12.0 software, the optimal working parameter combination obtained is a vibration frequency of 6 Hz, a crank speed of 204 r/min, and a lead screw feed speed of 15 mm/s. At this point, the predicted threshing efficiency is 94.9%, and the damage percentage is 3.5%.

The verification experiment was conducted in the laboratory of the College of Engineering at Shenyang Agricultural University. The working parameters of the root-soil separation test bench of Gentian were set to a vibration frequency of 6 Hz, a crank speed of 204 r/min, and a lead screw feed speed of 15 mm/s. The experiment was carried out a total of 8 times, and the results were averaged.

The average threshing efficiency of the *Gentiana* root system was 90.8%, and the average damage percentage was 5.9%. Compared with the simulation test, the relative errors were 4.1% and 2.4%, respectively. The root-soil separation effect was good. The threshing efficiency in the test bench experiment was slightly lower, but the result difference was within a reasonable range, indicating that the regression model has good reliability.

CONCLUSIONS

1) This paper addresses the existing problem of difficulty in separating *Gentiana* roots from soil, and designs a root-soil separation device of *Gentian*, which mainly includes a striking mechanism, a vibration mechanism, and an adjustable reciprocating mechanism. The crank-slider mechanism is used to drive the striking and vibration mechanisms, and the ball screw mechanism is used to drive the adjustable reciprocating mechanism to complete the root-soil separation operation.

2) Kinematic analysis of the striking mechanism is conducted to obtain a crank speed range of 168 r/min ≤ n ≤ 240 r/min. The forces acting on RSCG on the vibrating screen are analyzed to determine the vibration frequency range of the vibrating screen to be 4 Hz~8 Hz. Based on the early impact tests, the average height difference of RSCG was determined. Taking the midpoint of the crank speed, the operating speed range of the adjustable reciprocating mechanism was set to 10~20 mm/s.

3) The Box-Behnken response surface optimization test method is used to analyze the effects of vibration frequency, crank speed, and screw feed speed on the threshing efficiency and damage percentage, to establish a regression model, and to analyze their interactions. Finally, a multi-objective optimization design of the regression model for the test indicators is carried out, and the optimal working parameters combination is determined to be: vibration frequency 6 Hz, crank speed 204 r/min, screw feed speed 15 mm/s. Verification tests are conducted with these parameters, and the *Gentiana* root system threshing efficiency is found to be 90.8%, and the damage percentage is 5.9%. The relative errors compared to the theoretical optimization results are both less than 5%, indicating that the parameter optimization regression model is reliable.

ACKNOWLEDGEMENT

This research was mainly supported by the support of the Basic Scientific Research Program of the Education Department of Liaoning Province (LJKMZ20220998). National Natural Science Foundation of China (52275264). The authors thank relevant scholars for their assistance in the literature.

REFERENCES

[1] Chen Xueshen, Ma Xu, Chen Guorui, Qi Long, Wu Tao, Zeng Lingchao. (2015), Research on soil-rhizome separating device of deep-rhizome Chinese herbal medicines (深根茎类中药材根土分离装置的研究), *Mechanical Design*, vol.32, no.7, pp.65-70.

[2] Cui Zhenmeng, Zhang Zhaoguo, Wang Fa'an, Cheng Yiqi, Yang Haihui, Yang Yating, Gao Qingsheng. (2018), Kinematic analysis and optimization design of vibration-type device for panax notoginseng root-

soil separation (振动式三七根土分离装置的运动学分析及优化设计), *Journal of Northwest Agriculture and Forestry University (Natural Science Edition)*, vol.46, no.11, pp.146-154.

[3] Cui Zhichao, Guan Chunsong, Xu Tao, Fu Jingjing, Chen Yongsheng, Gao Qingsheng. (2021). Design and experiment of transplanting machine for cabbage substrate block seedlings, *INMATEH-Agricultural Engineering*, vol.64, no.2, pp.375-384.

[4] Gao Song, Sun Wensong, Wen Jian, Li Xiaoli, Yang Zhengshu, Li Ling. (2020), Diversity of Rhizosphere Bacterial and Function Predicted Analysis in Gentiana scabra Replanting Soil (连作龙胆草根际土壤细菌多样性及功能预测分析), *Journal of Shenyang Agricultural University*, vol.52, no.1, pp.102-108.

[5] Feng Xin, Wang Lijun, Yu Kunmeng, Gao Yunpeng, Bi Shengying, Wang Bo. (2023), Design and Experiment of Mechanism of Wave Screen for Maize Grain Cleaning (玉米籽粒清选波浪筛机构设计与试验), *Transactions of the Chinese Society for Agricultural Machinery*, vol.54, no.4, pp.142-154.

[6] Li Dongjie, Hou Jialin, Wang Dongwei, Chang Zengcun. (2024). Design and testing of peanut sieving prototype machine, *INMATEH-Agricultural Engineering*, vol.73, no.2, pp.760-770.

[7] Liu Yafeng, Fang Zhichao, Xia Haifeng, Qu Yongbo, Wu Mingliang. (2024), Design and Experiment of a Opposite Roller Extrusion Type Allium Chinese Harvester (对辊拨刷式藠头收获机设计与试验), *Journal of Agricultural Science and Technology*, vol.26, no.6, pp.72-81.

[8] Liu Zhixin, Shang Shuqi, Ma Shikuan, Hou Yaxiu, Dong Tongtong, He Xiaoning. (2024). Optimisation by coupled RECURDYN-EDEM simulation: Optimisation tests of a three-stage low-loss separation device for potato soil, *INMATEH-Agricultural Engineering*, vol.72, no.1, pp.138-147.

[9] Lu Dequan,Liu Qingliang,Mao Hongwei. (2022), The Design and Simulation Analysis of Impact Sampler for Deep Sea Mineral Deposit (深海矿床冲击式破碎器的结构设计及仿真分析), *Journal of Ocean Technology*, vol.41, no.1, pp.84-91.

[10] Luo Wei, Wang Jikui, Niu Hailong, Luo XinYu, Burlen·Halembek, Duan Wenxian, Li Yang. (2018), Design and Test on Debris Clean-up Device of Clamping Finger-chain Type Device for Recycling Agricultural Plastic Film (夹指链式残膜回收机清杂装置的设计与试验), *Journal of Agricultural Mechanization Research*, vol.40, no.2, pp.75-79.

[11] Lv Jinqing,Yang Xiaohan,Lv Yining, Li Zihui, Li Jicheng, Du Changlin (2022) Analysis and Experiment of Potato Damage in Process of Lifting and Separating Potato Excavator (马铃薯挖掘机升运分离过程块茎损伤机理分析与试验), *Transactions of the Chinese Society for Agricultural Machinery*, vol.51, no.1, pp.103-113.

[12] Qian Zhenjie; Zhang Dingguo. (2015), Frictional impact dynamics of flexible manipulator arms (含摩擦碰撞柔性机械臂动力学研究), *Journal of Vibration Engineering*, vol.28, no.6, pp.879-886.

[13] Quan Longzhe, Zhang Dan, Zeng Baigong, Tong Jin, Chen Donghui. (2013), Modeling and optimizing dither mechanism for conveying corn stubble (玉米根茬抖动升运机构的建模与优化) *Transactions of the Chinese Society of Agricultural Engineering*, vol.29, no.3, pp.23-29.

[14] Tao Guixiang, Zhang Ziheng,Yi Shujuan, Xia Chunlong, Ma Yongcai. (2022), Design and Test of Combined Swing Radix isatidi Root-soil Separation Device (板蓝根收获机组合筛面摆动式根土分离装置设计与试验), *Transactions of the Chinese Society for Agricultural Machinery*, vol.53, no.4, pp.109-119.

[15] Tang Yongfei, Zhao Yongman, Wang Jikui, Wang Zheng. (2020), Design and experiment of film removing device for clamping finger-chain type residual film collector (夹指链式残膜回收机脱膜装置设计与试验), *Transactions of the Chinese Society of Agricultural Engineering*, vol.36, no.13, pp.11-19.

[16] Wang Faan, Wen Bo, Xie Xiaohong, Xie Kaiting, Guo Siwei, Zhang Zhaoguo. (2023), Operation Mechanism Analysis and Parameter Optimization of Conveying and Separating Device of Panax notoginseng Harvester (三七收获机输送分离装置作业机理分析与参数优化), *Journal of Agricultural Machinery*, vol.54, no.S1, pp.201-211+259.

[17] Wei Zhongcai, Li Hongwen, Sun Chuanzhu, Li Xueqiang, Liu Wenzheng, Su Guoliang, Wang Faming. (2018), Improvement of potato harvester with two segment of vibration and wave separation (振动与波浪二级分离马铃薯收获机改进), *Transactions of the Chinese Society of Agricultural Engineering*, vol.34,no.12, pp.42-52.

[18] Wei Zhongcai, Li Hongwen,Su Guoliang, Sun Chuanzhu, Liu Wenzheng, Li Xueqiang. (2019), Development of potato harvester with buffer type potato-impurity separation sieve (缓冲筛式薯杂分离马铃薯收获机研制), *Transactions of the Chinese Society of Agricultural Engineering*, vol.35, no.8, pp.1-11.

[19] Wei Zhongcai,Wang Xinghuan,Li Xueqiang, Wang Faming, Li Zhihe, Jin Chengqian. (2023) Design and Experiment of Crawler Self-propelled Sorting Type Potato Harvester (履带自走式分拣型马铃薯收获机设计

与试验), *Transactions of the Chinese Society for Agricultural Machinery*, vol.54, no.2, pp.95-106.

[20] Xue Haotian. (2022), The Whole Machine Design and Simulation Test of Key Components of Panax notoginseng Combined Harvester (三七联合收获机整机设计及关键部件的仿真试验), *Kunming University of Science and Technology*.

[21] Yang Ranbing, Wu Minsheng, Xu Peng, Pan Yongfei, Lv Danyang, Zha Xiantao. (2024). Design and experiment of sweet potato combine harvester based on two-segment potato soil separation device, *INMATEH-Agricultural Engineering*, vol.74, no.3, pp.509-525.

[22] Yan Shuai, Cui Qingliang, Zhang Yanqing, Li Guang, Zhao Zhihong, An Nan. (2023), Design and testing of a drum-type root-soil separator for Codonopsis pilosula harvesting (党参收获滚筒式根土分离试验台的设计与试验), *Journal of Gansu Agricultural University*, vol.58, no.2, pp.226-234.

[23] Zhao Zhan, Li Yaoming, Chen Yi, Liang Zhenwei, Liu Lixia. (2013), Impact Mechanical Characteristics Analysis of Rice Grain (水稻籽粒碰撞力学特性研究), *Transactions of the Chinese Society for Agricultural Machinery*, vol.44, no.6, pp.88-92.

[24] Zou Yagang (2023) Mechanism Analysis and Parameter Optimization of Tea Shaking Screen Machine (茶叶抖筛机的机理分析与参数优化), *Anhui Agricultural University*.